

Synthetic spin-orbit coupling for the multi-spin models in optical lattices

Zhen Zheng,^{1,2,3,*} Yan-Qing Zhu,^{3,4} Shanchao Zhang,^{1,2,4} Shi-Liang Zhu,^{1,2,4,†} and Z. D. Wang^{3,4,‡}

¹Key Laboratory of Atomic and Subatomic Structure and Quantum Control (Ministry of Education), Guangdong Basic Research Center of Excellence for Structure and Fundamental Interactions of Matter, School of Physics, South China Normal University, Guangzhou 510006, China

²Guangdong Provincial Key Laboratory of Quantum Engineering and Quantum Materials, Guangdong-Hong Kong Joint Laboratory of Quantum Matter, Frontier Research Institute for Physics, South China Normal University, Guangzhou 510006, China

³Department of Physics and HK Institute of Quantum Science & Technology, The University of Hong Kong, Pokfulam Road, Hong Kong, China

⁴Quantum Science Center of Guangdong-Hong Kong-Macao Greater Bay Area, Shenzhen, China

The essential role of synthetic spin-orbit coupling in discovering new topological matter phases with cold atoms is widely acknowledged. However, the engineering of spin-orbit coupling remains unclear for arbitrary-spin models due to the complexity of spin matrices. In this work, we develop a more general but relatively straightforward method to achieve spin-orbit coupling for multi-spin models. Our approach hinges on controlling the coupling between distinct pseudo-spins through two intermediary states, resulting in tunneling with spin flips that have direction-dependent strength. The engineered spin-orbit coupling can facilitate topological phase transitions with Chern numbers over 1, a unique characteristic of multi-spin models compared to spin-1/2 models. By utilizing existing cold atom techniques, our proposed method provides an ideal platform for investigating topological properties related to large Chern numbers.

I. INTRODUCTION

Cold atoms exhibit quantum properties and statistics similar to traditional condensed-matter systems, yet confer the technical advantages of the artificial controllability [1–4]. It has been established as a clean and tunable platform to quantum simulate a variety of physics models that have attracted tremendous interests in cold atomic research of recent decades. Notably, the successful engineering and realization of the synthetic gauge fields using cold atoms [1, 2, 5, 6] has shed the light on exploring topological matters [7, 8]. Among these previous studies, the synthetic spin-orbit coupling (SOC) between atoms plays the crucial role because it provides a direct and simple routine to introduce the nontrivial Berry curvature to the system [1, 2, 9–12], which becomes the origin of the emergent topological phases.

In neutral atomic gases, SOC is proposed via a two-photon Raman process [13–15]. The atoms can acquire a net momentum transfer when transiting between the coupled internal states. If one interprets these internal states as the pseudo-spins, this transition will exhibit the form of an intrinsic gauge field that can emulate the SOC studied in the condensed-matter physics. Experimental investigations have reported the successful synthesis of SOC in atomic species including ⁸⁷Rb [16–26], ⁴⁰K [27, 28], ⁶Li [29], ⁸⁷Sr [30–32], ¹⁶¹Dy [33], ¹⁷³Yb [34–36] but not limited to these. Most of those achievements [37–39] and relative applications [15, 40–66] focus on the spin-1/2 model, which is composed of two pseudo-spins.

Hence the reported topological phases are usually characterized by Chern number that does not exceed 1. Beyond the spin-1/2 model, the multi-spin ones can bring in more topological properties. The protocol for synthesizing SOC is thus desirable for exploring these systems, but only the spin-1 model is investigated to date [67–76]. An intuitive scheme is to add more optical fields to couple the additional pseudo-spins. However the complexity of spin matrices in multi-spin systems frustrates the manipulations to these fields, hence it remains elusive so far in obtaining the desired SOC.

Here in this paper, we propose a general scheme for realizing SOC in systems with arbitrary pseudo-spins trapped in optical lattices. The proposal is based on involving two inter-mediate states that bridge the transition between different pseudo-spins, leading to an effective gauge field whose strength is locked to the tunneling direction. As the results, the SOC is generated simply by one optical field without introducing additional fields. After applying SOC in the two-dimensional (2D) system, we find rich topological transitions associated with large Chern number, which are the unique feature of the multi-spin models. Therefore this proposal can offer the feasible way for exploring and detecting topological properties for the multi-spin models.

The paper is organized as follows. In Sec. II, we present the model Hamiltonian of focus. We show the engineering of the effective SOC by introducing two intermediate states to couple two pseudo-spins. In Sec. III, we extend the results of the one-dimensional (1D) model to the 2D case. The engineered SOC can exhibit various forms under the artificial manipulations. Such a system hosts topological phases as well as topological edge modes, and the results are discussed in Sec. IV. We discuss the potential experimental implements of this proposal in Sec. V.

* zhenzhen@m.scnu.edu.cn

† slzhu@scnu.edu.cn

‡ zwang@hku.hk

Finally, we summarize the work in Sec.VI.

II. MODEL HAMILTONIAN

We start from the cold atomic gases with two manifolds of internal states. The atomic level structure is illustrated in FIG.1(a). We label the level manifold with the lower energy as the ground states $|g_\sigma\rangle$, and the other one with the higher energy as the excited states $|e_\sigma\rangle$. Each manifold is composed of quasi-spins labeled as $\sigma = 1, 2, \dots, N_s$ with N_s denoting the number of quasi-spins. To establish a simple physics picture of our proposal, we firstly deal with the 1D case. The two level manifolds are respectively loaded into two sets of optical lattices with the trap potentials as $V_{OL,g}(x) = V_L \cos^2(k_L x)$ and $V_{OL,e}(x) = V_L \sin^2(k_L x)$. Here V_L denotes the trap depth and $k_L = \pi/d$ with d denoting the lattice constant. We assume $\hbar = 1$ in the whole paper. Such a setup consists in a superlattice structure shown in FIG.1(b), in which each $|e\rangle$ site resides in the center of two adjacent $|g\rangle$ sites. Thereby the unit cell is composed of two sites that belong to different sublattices.

We consider the following Hamiltonian,

$$H = \sum_{\sigma} \hat{H}_{\sigma} + \hat{H}_{oc}. \quad (1)$$

The first part, i.e. Hamiltonian of the spin- σ atoms, in the free space is expressed as follows,

$$\begin{aligned} \hat{H}_{\sigma} = & \int dx \sum_{\lambda=g,e} \psi_{\lambda\sigma}^{\dagger}(x) \left[-\frac{\nabla_x^2}{2m} - \mu + V_{OL,\lambda}(x) \right] \psi_{\lambda\sigma}(x) \\ & + \Gamma \psi_{e\sigma}^{\dagger}(x) \psi_{e\sigma}(x). \end{aligned} \quad (2)$$

Here $\psi_{\lambda\sigma}$ and $\psi_{\lambda\sigma}^{\dagger}$ stands for the annihilation and creation operators of the $|\lambda_{\sigma}\rangle$ ($\lambda = g, e$) atoms. μ is the chemical potential. m denotes the atomic mass. Γ stands for the relative energy detuning of $|e\rangle$ with respect to $|g\rangle$ during the level transition described in the next texts.

To engineer the Hamiltonian of interests, we generate the optical coupling between the g and e sublattices by using the field Ω_1 , which undergoes the transitions from $|g_{\sigma}\rangle$ to $|e_{\sigma}\rangle$ within the same pseudo-spin. Besides, a spin-flip term is also introduced via a spatially modulated field Ω_2 that only couples pseudo-spins of $|e\rangle$. The level transitions are shown in FIG.1(a). It gives the form of the second part of Hamiltonian (1),

$$\hat{H}_{oc} = \int dx \sum_{\sigma=1}^{N_s} \Omega_1 \psi_{e\sigma}^{\dagger} \psi_{g\sigma} + \sum_{\sigma=1}^{N_s-1} \hat{\Omega}_2(x) \eta_{\sigma} \psi_{e\sigma}^{\dagger} \psi_{e,\sigma+1} + H.c. \quad (3)$$

Here $\hat{\Omega}_2(x)$ denotes the spatially modulated mode of the Ω_2 field. η_{σ} is the coefficient dependent on the particular transition from $|e_{\sigma}\rangle$ to $|e_{\sigma+1}\rangle$ ($\sigma = 1, 2, \dots, N_s - 1$), and we will discuss its form later. $H.c.$ stands for the Hermitian conjugation.

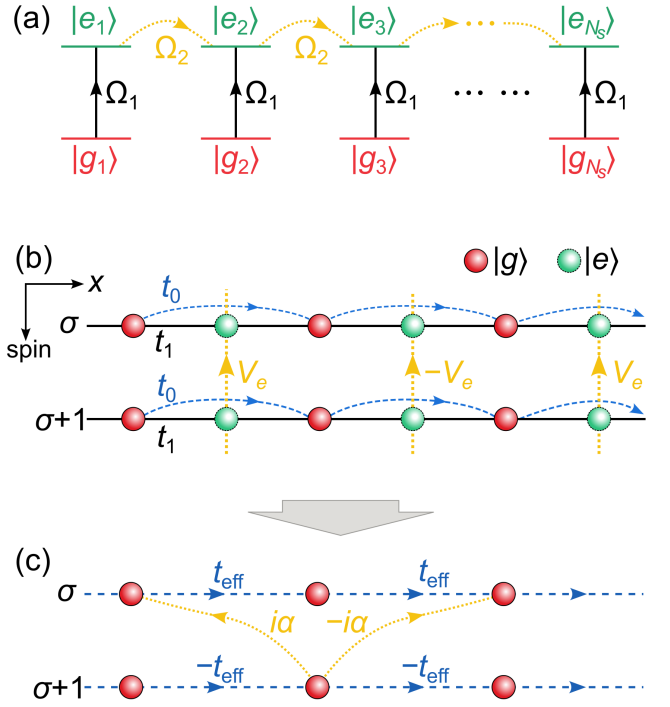


FIG. 1. (a) Setups of the atomic level transitions. $|g_{\sigma}\rangle$ and $|e_{\sigma}\rangle$ are coupling by the field Ω_1 (black solid lines), while $|e_{\sigma}\rangle$ and $|e_{\sigma+1}\rangle$ are coupled by the field Ω_2 (yellow dotted lines). (b) Illustration of the 1D lattice model. The lattice is composed of N_s chains specified by the pseudo-spin index. For each chain, the atoms of $|e_{\sigma}\rangle$ are loaded in the center of two adjacent atoms of $|g_{\sigma}\rangle$. The transitions driven by Ω_1 in (a) generate intra-chain coupling t_1 (black solid lines), and the ones driven by Ω_2 generate the inter-chain coupling V_e (yellow dotted lines) but in a staggered pattern in the x direction. (c) The mapped lattice model after adiabatically eliminating $|e_{\sigma}\rangle$. It gives rises to effective SOC (yellow dotted lines) for atoms of $|g\rangle$.

To capture the physics of the lattice model, we use the tight-binding approximation, and expand the atomic operator in terms of the Wannier wave function: $\psi_{\lambda\sigma}(x) = \sum_j W(x - x_j) \psi_{j\lambda\sigma}$, where x_j denotes the coordinate of the j -th site. Then the model Hamiltonian (1) is written as

$$H = H_0 + H_1 + H_2. \quad (4)$$

The first part of Eq.(4) originates from Hamiltonian (2),

$$\begin{aligned} H_0 = & - \sum_{\langle i,j \rangle} \sum_{\lambda,\sigma} t_0 \psi_{i\lambda\sigma}^{\dagger} \psi_{j\lambda\sigma} - \sum_{j,\lambda,\sigma} \mu \psi_{j\lambda\sigma}^{\dagger} \psi_{j\lambda\sigma} \\ & + \sum_{j,\sigma} \Gamma \psi_{je\sigma}^{\dagger} \psi_{je\sigma}, \end{aligned} \quad (5)$$

where the summation $\sum_{\langle i,j \rangle}$ takes over all the nearest-neighbor sites, and t_0 is the tunneling magnitude.

The second part of Eq.(4) describes the coupling between the g and e sublattices. Notice that due to the

spatial offset between the g and e sublattices, each $|g\rangle$ atoms is coupled to two $|e\rangle$ atoms on its adjacent sites. Hence H_1 is expressed as

$$H_1 = \sum_{j\sigma} t_1 (\psi_{j,e,\sigma}^\dagger + \psi_{j+1,e,\sigma}^\dagger) \psi_{j,g,\sigma} + H.c., \quad (6)$$

where $t_1 = \Omega_1 \int W^*(x+d/2)W(x)dx$.

The last part of Eq.(4) describes the spin-flip field of the e sublattice. Practically, its spatial modulated mode can be prepared as $\hat{\Omega}_2(x) = \Omega_2 \cos(k_L x)$. Since the Wannier wave function $W(x)$ is of even parity with respect to the site center, H_2 is expressed as

$$H_2 = \sum_j \sum_{\sigma=1}^{N_s-1} (-1)^j \hat{V}_e \eta_\sigma \psi_{j,e,\sigma}^\dagger \psi_{j,e,\sigma+1} + H.c., \quad (7)$$

where the magnitude of the spin-flip field is $\hat{V}_e = \Omega_2 \int \cos(k_L x) |W(x)|^2 dx$. Notice that in Eq.(7), the spatial modulation of the spin-flip term is exhibited as a staggered pattern. This is ascribed to the $2d$ periodicity of $\hat{\Omega}_2(x)$. It indicates that the atom will undergo a momentum transfer of k_L when flipping its spin. Such a modulation plays the crucial role in generating SOC which will be seen later.

In the momentum k_x space, due to the spatial modulation of Hamiltonian (7), we choose the basis $\Psi_{k_x} = (\Phi_{k_x,g}, \Phi_{k_x,e})^T$, where $\Phi_{k_x,\lambda} = (\psi_{k_x,\lambda,1}, \psi_{k_x+k_L,\lambda,2}, \dots, \psi_{k_x+(N_s-1)k_L,\lambda,N_s})$. Then Hamiltonian (4) is recast as

$$\mathcal{H}(k_x) = \begin{pmatrix} \hat{H}_g & \hat{V} \\ \hat{V}^\dagger & \hat{H}_e \end{pmatrix}, \quad (8)$$

where the block-diagonal terms are

$$\begin{aligned} \hat{H}_g(k_x) &= \xi_{k_x} \sigma_z - \mu \sigma_0, \\ \hat{H}_e(k_x) &= \hat{H}_g + \Gamma + \hat{V}_e \mathcal{M} + \hat{V}_e^* \mathcal{M}^\dagger, \end{aligned}$$

and the block-off-diagonal term is

$$\hat{V}(k_x) = \text{Diag}[t_1 + t_1 e^{ik_x d}, \dots, t_1 + (-1)^{N_s-1} t_1 e^{ik_x d}].$$

Here $\sigma_{x,y,z,0}$ are the Pauli matrices defined in the spin space. $\xi_{k_x} = -2t_0 \cos(k_x d)$. The nonzero elements of the matrix \mathcal{M} are

$$\mathcal{M}_{\sigma,\sigma+1} = \eta_\sigma \quad (9)$$

for $\sigma = 1, 2, N_s - 1$, otherwise $\mathcal{M}_{\sigma,\sigma'} = 0$.

We assume that the atoms are initially prepared in $|g\rangle$ and far detuned from $|e\rangle$, yielding that $|e\rangle$ can be adiabatically eliminated. The effective Hamiltonian is then obtained by $\mathcal{H}_{\text{eff}}(k_x) = \hat{H}_g + \hat{V}(\hat{H}_g - \hat{H}_e)^{-1} \hat{V}^\dagger$ from Hamiltonian (8) (see Appendix A), which gives

$$\mathcal{H}_{\text{eff}}(k_x) = \xi_{k_x} \mathcal{M}_z - \mu + \hat{\zeta}_{k_x} + (\hat{\alpha}_{k_x} \hat{V}_e \mathcal{M} + H.c.). \quad (10)$$

Here \hat{V}_e is set as $\hat{V}_e = V_e e^{i\varphi_e}$ with φ_e denoting its phase, $\mathcal{M}_z = \text{Diag}[1, -1, 1, -1, \dots]$, $\hat{\zeta}_{k_x} = \text{Diag}[\hat{\zeta}_1(k_x), \dots, \hat{\zeta}_{N_s}(k_x)]$, and

$$\begin{cases} \hat{\zeta}_\sigma(k_x) = -\frac{\Gamma}{\Gamma^2 - V_e^2} t_1^2 |1 - (-1)^\sigma e^{ik_x d}|^2 \\ \hat{\alpha}_{k_x} = -\frac{V_e e^{i\varphi_e}}{\Gamma^2 - V_e^2} t_1^2 (1 + e^{ik_x d})(1 - e^{-ik_x d}) \end{cases}.$$

Hamiltonian (10) can be further written in a compact form,

$$\mathcal{H}_{\text{eff}}(k_x) = \xi_{\text{eff}}(k_x) \mathcal{M}_z - \mu_{\text{eff}} + \mathcal{H}_{\text{soc}}(k_x), \quad (11)$$

$$\mathcal{H}_{\text{soc}}(k_x) = -2\alpha V_e \sin(k_x d) (i e^{i\varphi_e} \mathcal{M} + H.c.). \quad (12)$$

Here $\xi_{\text{eff}}(k_x) = -2t_{\text{eff}} \cos(k_x d)$, $t_{\text{eff}} = t_0 + \zeta/2$ with $\zeta = 2t_1^2 \Gamma / (\Gamma^2 - V_e^2)$ is the effective tunneling magnitude, $\mu_{\text{eff}} = \mu + \zeta$ is the effective chemical potential, and

$$\alpha = \frac{t_1^2 V_e}{\Gamma^2 - V_e^2}. \quad (13)$$

From Eq.(11), we can see the final effective Hamiltonian is now assigned with the α term. Such a term describes a nearest-neighbor tunneling process associated with the spin flip, and the sign of the tunneling magnitude is locked to tunneling direction. Hence the tunneling process indeed exhibits the physics picture of SOC. For the spin-1/2 case simply with $\eta_\sigma = 1$ in Eq.(9), it gives rise to $\mathcal{H}_{\text{soc}} = 2\alpha \sin(k_x d) \sigma_y$ when $\varphi_e = 0$ and $\mathcal{H}_{\text{soc}} = -2\alpha \sin(k_x d) \sigma_x$ when $\varphi_e = \pi/2$, where $\sigma_{x,y,z}$ denotes the Pauli matrix. For the general case with N_s spins, the spin matrices will have complex forms beyond the Pauli matrices as $S_z = \text{Diag}[-S, -S+1, \dots, S]$ with $S = (N_s - 1)/2$, and $S_{x,y}$ are derived by the matrix representation of the raising and lowering operators S_\pm , reading $S_x = (S_+ + S_-)/2$ and $S_y = (S_+ - S_-)/(2i)$. Here the nonzero elements of the S_\pm matrices are given by $[S_\pm]_{\sigma\pm 1, \sigma} = \frac{1}{2} \sqrt{S(S+1) - (\sigma - S - 1)(\sigma - S)}$. Therefore, intuitively by preparing $\mathcal{M} = S_-$ using additional optical fields, we can obtain the generalized form of SOC for systems with N_s spins. However, it suffers from the complexity of the spin matrices to deliberately tune the coupling driven by various optical fields. We will discuss this issue in Sec.V.

In Eq.(13), the synthetic SOC is composed of two parts as $i e^{i\varphi_e} = i \cos(\varphi_e) - \sin(\varphi_e)$. It reveals that the two parts have a relative $\pi/4$ phase, and their relative strength of can be controllable by changing φ_e . Since engineered by adiabatically eliminating two intermediate $|e\rangle$ states, the engineered SOC indeed originates from a third-order perturbative process with respect to Hamiltonian (5), which can be also recognized by the form of Eq.(13). Therefore the SOC strength depends on not only the g - e coupling t_1 but also the staggered spin-flip field V_e . This facilitates the artificial controllability to the engineered SOC. We note that in obtaining Eq.(10), we have made the assumption of far detuning. This yields $\Gamma > V_e$, hence α in Eq.(13) is positive.

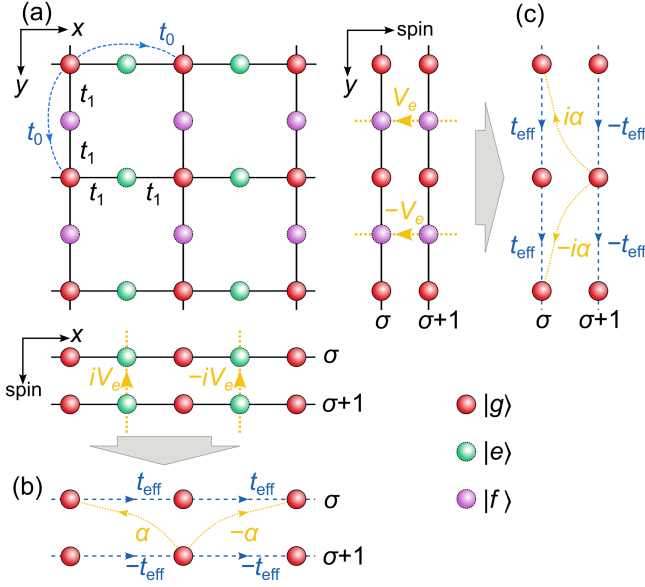


FIG. 2. (a) Illustration of the 2D lattice model. The lattice is composed of N_s planes specified by the pseudo-spin index. For each plane, the atoms of $|e\rangle$ (or $|f\rangle$) are loaded in the center of two adjacent atoms of $|g\rangle$ in the x (or y) direction. (b)-(c) The mapped lattice models after adiabatically eliminating $|e\rangle$ and $|f\rangle$, and projecting in the x and y directions. It gives rise to effective SOC (yellow dotted lines) of which the strength and phase can be separately controlled in the x and y directions. Here we show the example of the Rashba SOC.

III. 2D CASE

The proposal can be extended to the 2D lattice model, which can result in a variety of SOC with rich forms. To individually manipulating SOC in different spatial dimensions, a third manifolds of excited states $|f_\sigma\rangle$ is necessary, and thereby the extended atomic level transitions are illustrated in FIG.2. The lattice potential is accommodated correspondingly: the $|e\rangle$ atoms reside in the center of two adjacent g sites along the x direction, by contrast the $|f\rangle$ atoms reside in the similar pattern but along the y direction. They lead to a Lieb superlattice structure, which is shown in FIG.2(a).

We process the same derivations as formulated in Sec.II. After adiabatically eliminating $|e\rangle$ and $|f\rangle$, the effective Hamiltonian is written in the same form of Eq.(11) as,

$$\mathcal{H}_{\text{eff}}(\mathbf{k}) = \xi_{\text{eff}}(\mathbf{k})\mathcal{M}_z - \mu_{\text{eff}} + \mathcal{H}_{\text{soc}}(\mathbf{k}), \quad (14)$$

where $\xi_{\text{eff}}(\mathbf{k}) = -2t_{\text{eff}}[\cos(k_x d) + \cos(k_y d)]$, and SOC for the 2D case is presented as

$$\begin{aligned} \mathcal{H}_{\text{soc}}(\mathbf{k}) = & -i2\alpha V_e \sin(k_x d) e^{i\varphi_e^{(x)}} \mathcal{M} \\ & - i2\alpha V_e \sin(k_y d) e^{i\varphi_e^{(y)}} \mathcal{M} + H.c. \end{aligned} \quad (15)$$

Practically, $\varphi_e^{(x)}$ and $\varphi_e^{(y)}$ can be separately tuned. By

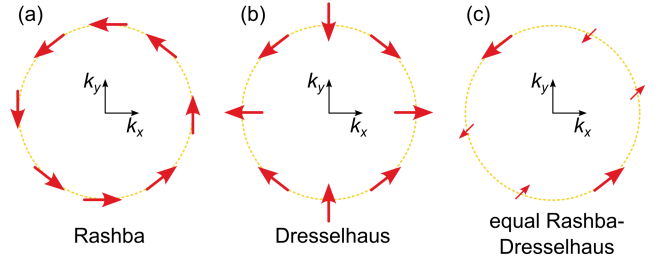


FIG. 3. Illustration of the spin texture in the momentum space generated by (a) Rashba, (b) Dresselhaus, and (c) equal Rashba-Dresselhaus SOC. The pseudo-spin orientation is shown by the red arrows, whose length indicates the magnitude.

preparing $\mathcal{M} = S_-$ as discussed in Sec.II, one can obtain (i) the Rashba SOC [77] by setting $(\varphi_e^{(x)}, \varphi_e^{(y)}) = (0, \pi/2)$,

$$\mathcal{H}_{\text{soc}}^{(R)}(\mathbf{k}) = 2\alpha V_e [\sin(k_x d) S_y - \sin(k_y d) S_x], \quad (16)$$

(ii) the Dresselhaus SOC [78] by setting $(\varphi_e^{(x)}, \varphi_e^{(y)}) = (-\pi/2, \pi)$,

$$\mathcal{H}_{\text{soc}}^{(D)}(\mathbf{k}) = 2\alpha V_e [\sin(k_x d) S_x - \sin(k_y d) S_y], \quad (17)$$

and (iii) the equal Rashba-Dresselhaus SOC by setting $(\varphi_e^{(x)}, \varphi_e^{(y)}) = (-\pi/4, 3\pi/4)$,

$$\mathcal{H}_{\text{soc}}^{(RD)}(\mathbf{k}) = \frac{1}{\sqrt{2}} [\mathcal{H}_{\text{soc}}^{(R)}(\mathbf{k}) + \mathcal{H}_{\text{soc}}^{(D)}(\mathbf{k})]. \quad (18)$$

The above three types of SOC exhibit various patterns in the spin texture, which are illustrated in FIG.3. Intriguing topological properties can arise from these non-trivial spin texture structure.

IV. BAND TOPOLOGY

It has been known that the band inversion in accompany of SOC can support the topological phase transition from the trivial to non-trivial gapped phases. Specifically in 2D case, this is known to be captured by the quantized Chern number as the topological invariant [79],

$$\mathcal{C} = \sum_{n \in \text{occ}} \mathcal{C}_n, \quad (19)$$

where the n 's summation takes over all the occupied (abbreviated as occ) bands, and \mathcal{C}_n is the Chern number of the n -th band calculated as

$$\mathcal{C}_n = \frac{1}{2\pi} \int_{\text{BZ}} \mathcal{A}_n(\mathbf{k}) d\mathbf{k}.$$

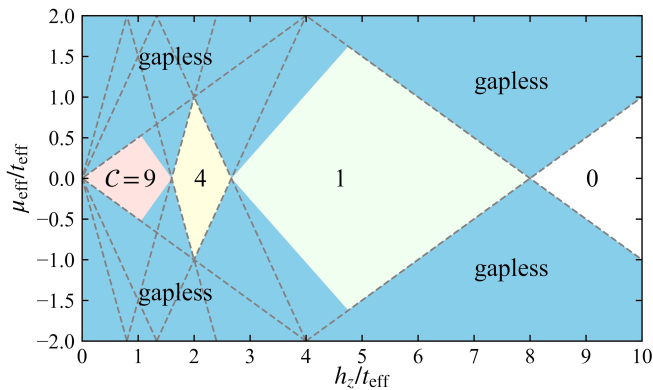


FIG. 4. Phase diagram for the 2D model with $N_s = 6$ and Rashba SOC. The number denotes the Chern number \mathcal{C} of each phase. The blue regions outline the gapless phase. The grey-dashed lines correspond to the gap-closing condition indicated by Eq.(21). We set $\alpha = 1.2t_{\text{eff}}$.

Here BZ stands for the Brillouin zone. $\mathcal{A}_n(\mathbf{k})$ is the Berry curvature of the n -th band formulated as

$$\mathcal{A}_n(\mathbf{k}) = i \sum_{m \neq n} \frac{\langle n | \nabla_{k_x} \hat{H} | m \rangle \langle m | \nabla_{k_y} \hat{H} | n \rangle}{E_n(\mathbf{k}) - E_m(\mathbf{k})} - (k_x \leftrightarrow k_y).$$

$|n\rangle$ and $E_n(\mathbf{k})$ denotes the eigen-state and eigen-energy of the n -th band for the Hamiltonian \hat{H} .

Notice that in the effective Hamiltonian (14), the matrix \mathcal{M}_z is not identical to S_z , and hence the system is gapless. Since \mathcal{C} is only well defined in a gapped system, we introduce a additional Zeeman term with the strength h_z into the effective Hamiltonian (14),

$$\hat{H}(\mathbf{k}) = \mathcal{H}_{\text{eff}}(\mathbf{k}) + h_z S_z. \quad (20)$$

Hereafter for simplicity without loss of generality, we consider the $N_s = 6$ model with the Rashba SOC in \mathcal{H}_{eff} , see Eq.(16). In experiments, this Zeeman term can be naturally present by the Zeeman splitting or the energy offset for the pseudo-spin states. We plot the phase diagram in the h_z - μ_{eff} plane. At $\mu_{\text{eff}} = 0$, by increasing h_z , \mathcal{C} processes the changes from 9, 4, 1, to 0. It reveals that the transitions occur within three topological phases with nonzero \mathcal{C} . When $\mu_{\text{eff}} \neq 0$, the topological phases are separated by the gapless phase. We remark that the phenomenon associated with the emergent large \mathcal{C} is the feature of the multi-spin models that is distinct from the spin-1/2 one [79], because \mathcal{C} is limited by its maximum N_s .

Generally, the topological phase transitions are in accompany with the closing and reopening of the band gaps. To extract a clear picture of the topological transitions with large \mathcal{C} , we calculate the gap characterized by the quantity $\Delta_g = \min(|E_n(\mathbf{k})|)$ and plot it as the function of h_z in FIG.5(a). We find Δ_g vanishes at the critical points during the topological phase transitions.

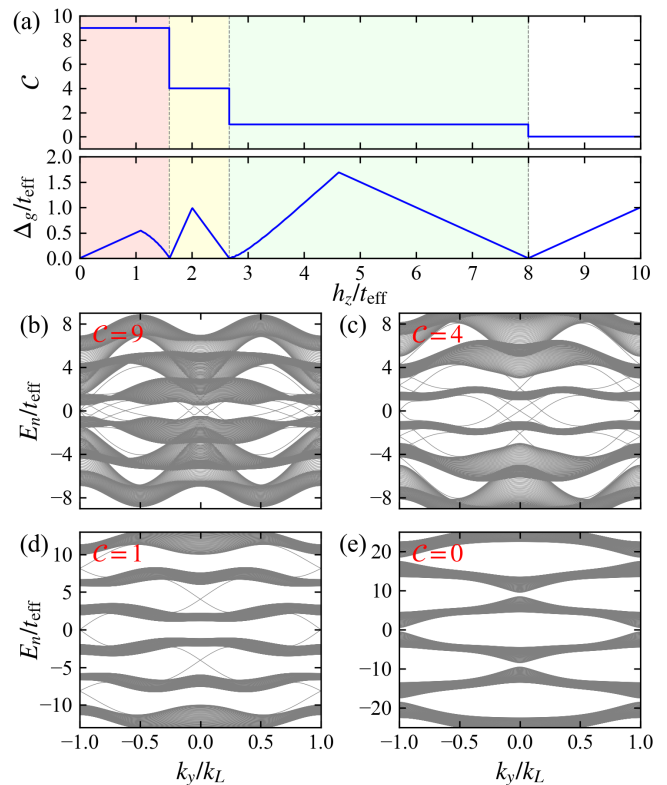


FIG. 5. (a) The Chern number \mathcal{C} and gap Δ_g as functions of h_z . The grey dashed lines mark the critical points of the phase transitions. We set $\mu_{\text{eff}} = 0$ and $\alpha = 1.2t_{\text{eff}}$. (b)-(e) Spectrum of the system with the cylindrical geometry for $h_z = 1t_{\text{eff}}$ (b), $2t_{\text{eff}}$, $4t_{\text{eff}}$ (d), and $9t_{\text{eff}}$ (e). The value of the Chern number \mathcal{C} is shown in each panel. Other parameters are the same with (a).

yielding that the band gap closes and reopens. In Hamiltonian (20), the band only closes at $\mathbf{k}_c = (k_c, k_c)$ with $k_c = 0, \pm k_L$, i.e. at the center or corners of BZ. It indicates that α does not affect the gap closing, and thus we do not further inspect the influence of its magnitude on the topological transition. The phase boundaries are intuitively determined by assuming that one of diagonal terms in Eq.(20) vanishes. It gives the following equation,

$$|K_1 t_{\text{eff}} - \mu_{\text{eff}} \pm h_z K_2 / 2| = 0, \quad (21)$$

where the integers $K_1 = 0$ or ± 4 , and $K_2 = 1, 3$, or 5 . Particularly at $\mu_{\text{eff}} = 0$, it gives rise to the phase boundaries at $h_z/t_{\text{eff}} = 0, \frac{8}{5}, \frac{8}{3}, 8$. This result has been verified in FIG.5(a). When $\mu_{\text{eff}} \neq 0$, several phase boundaries deviate from the prediction of Eq.(21), as shown in FIG.4. This is because one of six bands is partially filled when increasing μ_{eff} under the the complex band structure, hence the system turns to the gapless phase.

As the topological phases support topological edges modes existed in the band gaps, we plot the spectrum in FIG.5(b)-(e). We use the cylindrical geometry by

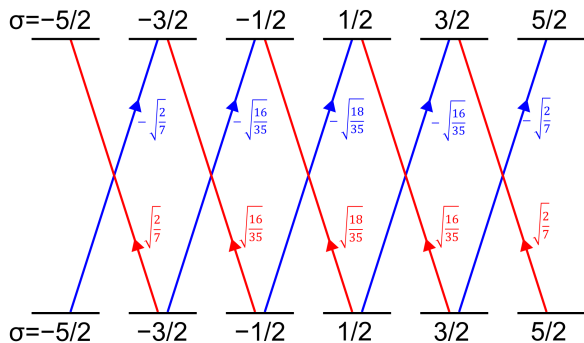


FIG. 6. Transitions between the pseudo-spins for the spin-5/2 model. The blue and red arrows describe the σ^+ and σ^- polarization process. The number beside each arrow indicates the Clebsch-Gordan coefficients during the transitions.

setting the open boundary condition in the x direction, while periodic boundary condition in the y direction. According to the bulk-edge correspondence, the number of the existing chiral edge modes is closely tied to \mathcal{C} [79]. We calculate \mathcal{C}_n for each band, and obtain $\mathcal{C}_n = \{1, 3, 5, -5, -3, -1\}$ from the bottom to top bands for panel (b), $\mathcal{C}_n = \{1, 3, 0, 0, -3, -1\}$ for panel (c), $\mathcal{C}_n = \{1, 0, 0, 0, 0, -1\}$ for panel (d), and $\mathcal{C}_n = 0$ for panel (e). As defined in Eq.(19), \mathcal{C} is given by summing \mathcal{C}_n of all the occupied bands. Therefore, in FIG.5(b)-(d), one can see that the number of zero-energy nodes in the spectrum is identical to \mathcal{C} (noting that the nodes are two-fold degenerate at $k_y = k_L$ in panel (b), and modes at $k_y = \pm k_L$ are equivalent due to the Bloch theorem).

V. EXPERIMENTAL IMPLEMENTS

In the above investigations, we use the $N_s = 6$ system as a concrete example to present the applications of the SOC in multi-spin models. A candidate system that can realize the model is the alkaline-earth-like atomic ensemble of ^{173}Yb [34]. Because its nuclear spin $I = 5/2$ provides $N_s = 2I + 1$ nuclear Zeeman states for both the ground $^1\text{S}_0$ and the meta-stable excited $^3\text{P}_0$ electronic states, which can be respectively selected to emulate $|g\rangle$ and $|e\rangle$. As discussed in Sec.II, the key to the synthetic SOC to preparing \mathcal{M} of Eq.(9) to share the form of the lowering operator S_- . Based on this scenario, we introduce the Ω_2 field in FIG.1(a) with the circular polarization to couple $|e_\sigma\rangle$ and $|e_{\sigma\pm 1}\rangle$. As the results, the coefficients η_σ in Eq.(9) can be represented by the Clebsch-Gordan coefficients during the transitions. This is sketched in FIG.6, from which one can find $\eta_\sigma \propto [S_-]_{\sigma-1,\sigma}$, and thus $\mathcal{M} \propto S_-$ up to a multiplicative constant. We remark that in this way, all the transitions can occur simultaneously by one optical field. It indicates that, compared with spin-1/2 one, the SOC for the multi-spin model can be generated without preparing additional fields.

VI. CONCLUSION

In summary, we have presented a scheme of synthesizing SOC for the multi-spin systems. A key of this proposal relies on manipulating the coupling of two intermediate states, which leads to a tunneling process between two pseudo-spins with the strength locked to the tunneling direction. A variety of SOC can be proposed in this way. They pave the way for exploring topological phases of the lattice models, and hence more topological edge modes characterized by the large Chern number may be discovered for such a multi-spin system.

ACKNOWLEDGMENTS

This work was supported by National Key R&D Program of China (Grant No. 2022YFA1405300), the National Natural Science Foundation of China (Grant No. 12074180), Innovation Program for Quantum Science and Technology (Grant No. 2021ZD0301700), the NSFC/RGC JRS grant (Grant No. N_HKU 774/21), GRF (Grants No. 17310622 and No. 17303023) of Hong Kong, and the Science and Technology Program of Guangzhou (Grant No. 2024A04J0004).

Appendix A: Effective Hamiltonian in the perturbation method

In this appendix we present the general derivations for obtaining the effective Hamiltonian using the perturbation method [80]. We consider a quantum system described by the state space $|\psi_1\rangle \oplus |\psi_2\rangle$ composed of two subspaces $|\psi_\lambda\rangle$ ($\lambda = 1, 2$). The physics of each subspace $|\psi_\lambda\rangle$ is governed by the Hamiltonian H_λ . V describes the coupling between the two subspaces. Generally, the subspace $|\psi_\lambda\rangle$ can be made up of several quantum states. Hence H_λ and V can be cast into the matrix representation. By choosing the basis $(|\psi_1\rangle, |\psi_2\rangle)^T$, the Hamiltonian of the system is written as

$$H = \begin{pmatrix} H_1 & V \\ V^\dagger & H_2 \end{pmatrix} \equiv H_0 + U. \quad (\text{A1})$$

where

$$H_0 = \begin{pmatrix} H_1 & \\ & H_2 \end{pmatrix}, \quad U = \begin{pmatrix} & V \\ V^\dagger & \end{pmatrix}. \quad (\text{A2})$$

Hereafter we regard the block-diagonal Hamiltonian H_0 as the unperturbative term, while the off-block-diagonal Hamiltonian U as the perturbative one. The Green's functions extracted from H and H_0 are defined as (with respect to the variable z)

$$G(z) = \frac{1}{z - H}, \quad G^{(0)}(z) = \frac{1}{z - H_0}. \quad (\text{A3})$$

Since H_0 is block-diagonal, its off-block-diagonal elements vanish. It reveals that

$$G_{12}^{(0)} = G_{21}^{(0)} = 0. \quad (\text{A4})$$

Likewise for U , we have

$$U_{11} = U_{22} = 0. \quad (\text{A5})$$

We aim to obtain the effective Hamiltonian for the $|\psi_1\rangle$ subspace of interests, yielding the $|\psi_2\rangle$ subspace is adiabatically eliminated. From the Dyson equation given as

$$G = G^{(0)} + G^{(0)}UG. \quad (\text{A6})$$

we only focus on the following block elements of the G

matrix,

$$G_{11} = G_{11}^{(0)} + G_{11}^{(0)}U_{12}G_{21}, \quad (\text{A7})$$

$$G_{21} = G_{22}^{(0)}U_{21}G_{11}. \quad (\text{A8})$$

Submitting G_{21} into G_{11} , we have

$$G_{11} = G_{11}^{(0)} + G_{11}^{(0)}U_{12}G_{22}^{(0)}U_{21}G_{11}. \quad (\text{A9})$$

The inverse of G_{11} gives

$$\begin{aligned} G_{11}^{-1} &= [G_{11}^{(0)}]^{-1}(1 - G_{11}^{(0)}U_{12}G_{22}^{(0)}U_{21}) \\ &= [G_{11}^{(0)}]^{-1} - U_{12}G_{22}^{(0)}U_{21}. \end{aligned}$$

Submitting Eq.(A3), we get

$$z - H_{\text{eff}} = z - H_1 - V \frac{1}{z - H_2} V^\dagger.$$

By replacing z by its first-order approximation $z \approx E_1$ with E_1 denoting the eigen-energy of H_1 , we obtain the effective Hamiltonian for the $|\psi_1\rangle$ subspace written as

$$H_{\text{eff}} \approx H_1 + V \frac{1}{E_1 - H_2} V^\dagger. \quad (\text{A10})$$

-
- [1] J. Dalibard, F. Gerbier, G. Juzeliūnas, and P. Öhberg, *Rev. Mod. Phys.* **83**, 1523 (2011).
- [2] D.-W. Zhang, Y.-Q. Zhu, Y. X. Zhao, H. Yan, and S.-L. Zhu, *Adv. Phys.* **64**, 253 (2018).
- [3] I. Bloch, J. Dalibard, and S. Nascimbène, *Nat. Phys.* **8**, 267 (2012).
- [4] C. Gross and I. Bloch, *Science* **357**, 995 (2017).
- [5] N. Goldman, G. Juzeliūnas, P. Öhberg, and I. B. Spielman, *Rep. Prog. Phys.* **77**, 126401 (2014).
- [6] A. Eckardt, *Rev. Mod. Phys.* **89**, 011004 (2017).
- [7] M. Z. Hasan and C. L. Kane, *Rev. Mod. Phys.* **82**, 3045 (2010).
- [8] X.-L. Qi and S.-C. Zhang, *Rev. Mod. Phys.* **83**, 1057 (2011).
- [9] V. Galitski and I. B. Spielman, *Nature* **494**, 49 (2013).
- [10] J. Zhang, H. Hu, X.-J. Liu, and H. Pu, in *Annual Review of Cold Atoms and Molecules*, Vol. 2 (World Scientific, Singapore, 2013) pp. 81–143.
- [11] H. Zhai, *Rep. Prog. Phys.* **78**, 026001 (2015).
- [12] S. Zhang and G.-B. Jo, *J. Phys. Chem. Solids* **128**, 75 (2019).
- [13] K. Osterloh, M. Baig, L. Santos, P. Zoller, and M. Lewenstein, *Phys. Rev. Lett.* **95**, 010403 (2005).
- [14] J. Ruseckas, G. Juzeliūnas, P. Öhberg, and M. Fleischhauer, *Phys. Rev. Lett.* **95**, 010404 (2005).
- [15] S.-L. Zhu, H. Fu, C.-J. Wu, S.-C. Zhang, and L.-M. Duan, *Phys. Rev. Lett.* **97**, 240401 (2006).
- [16] Y.-J. Lin, K. Jiménez-García, and I. B. Spielman, *Nature* **471**, 83 (2011).
- [17] C. Hamner, C. Qu, Y. Zhang, J. Chang, M. Gong, C. Zhang, and P. Engels, *Nat. Commun.* **5**, 4023 (2014).
- [18] A. J. Olson, S.-J. Wang, R. J. Niffenegger, C.-H. Li, C. H. Greene, and Y. P. Chen, *Phys. Rev. A* **90**, 013616 (2014).
- [19] X. Luo, L. Wu, J. Chen, Q. Guan, K. Gao, Z.-F. Xu, L. You, and R. Wang, *Sci. Rep.* **6**, 1 (2016).
- [20] Z. Wu, L. Zhang, W. Sun, X.-T. Xu, B.-Z. Wang, S.-C. Ji, Y. Deng, S. Chen, X.-J. Liu, and J.-W. Pan, *Science* **354**, 83 (2016).
- [21] J. Li, W. Huang, B. Shteynas, S. Burchesky, F. Ç. Top, E. Su, J. Lee, A. O. Jamison, and W. Ketterle, *Phys. Rev. Lett.* **117**, 185301 (2016).
- [22] F. A. An, E. J. Meier, and B. Gadway, *Sci. Adv.* **3**, 1602685 (2017).
- [23] J.-R. Li, J. Lee, W. Huang, S. Burchesky, B. Shteynas, F. Ç. Top, A. O. Jamison, and W. Ketterle, *Nature* **543**, 91 (2017).
- [24] W. Sun, B.-Z. Wang, X.-T. Xu, C.-R. Yi, L. Zhang, Z. Wu, Y. Deng, X.-J. Liu, S. Chen, and J.-W. Pan, *Phys. Rev. Lett.* **121**, 150401 (2018).
- [25] Z.-Y. Wang, X.-C. Cheng, B.-Z. Wang, J.-Y. Zhang, Y.-H. Lu, C.-R. Yi, S. Niu, Y. Deng, X.-J. Liu, S. Chen, and J.-W. Pan, *Science* **372**, 271 (2021).
- [26] Q.-X. Lv, Y.-X. Du, Z.-T. Liang, H.-Z. Liu, J.-H. Liang, L.-Q. Chen, L.-M. Zhou, S.-C. Zhang, D.-W. Zhang, B.-Q. Ai, H. Yan, and S.-L. Zhu, *Phys. Rev. Lett.* **127**, 136802 (2021).
- [27] L. Huang, Z. Meng, P. Wang, P. Peng, S.-L. Zhang, L. Chen, D. Li, Q. Zhou, and J. Zhang, *Nat. Phys.* **12**, 540 (2016).
- [28] Z. Meng, L. Huang, P. Peng, D. Li, L. Chen, Y. Xu, C. Zhang, P. Wang, and J. Zhang, *Phys. Rev. Lett.* **117**, 235304 (2016).

- [29] L. W. Cheuk, A. T. Sommer, Z. Hadzibabic, T. Yefsah, W. S. Bakr, and M. W. Zwierlein, *Phys. Rev. Lett.* **109**, 095302 (2012).
- [30] S. Kolkowitz, S. L. Bromley, T. Bothwell, M. L. Wall, G. E. Marti, A. P. Koller, X. Zhang, A. M. Rey, and J. Ye, *Nature* **542**, 66 (2017).
- [31] A. Aeppli, A. Chu, T. Bothwell, C. J. Kennedy, D. Kedar, P. He, A. M. Rey, and J. Ye, *Sci. Adv.* **8**, adc924 (2022).
- [32] M.-C. Liang, Y.-D. Wei, L. Zhang, X.-J. Wang, H. Zhang, W.-W. Wang, W. Qi, X.-J. Liu, and X. Zhang, *Phys. Rev. Res.* **5**, L012006 (2023).
- [33] N. Q. Burdick, Y. Tang, and B. L. Lev, *Phys. Rev. X* **6**, 031022 (2016).
- [34] L. F. Livi, G. Cappellini, M. Diem, L. Franchi, C. Clivati, M. Frittelli, F. Levi, D. Calonico, J. Catani, M. Inguscio, and L. Fallani, *Phys. Rev. Lett.* **117**, 220401 (2016).
- [35] B. Song, C. He, S. Zhang, E. Hajiyev, W. Huang, X.-J. Liu, and G.-B. Jo, *Phys. Rev. A* **94**, 061604 (2016).
- [36] B. Song, C. He, S. Niu, L. Zhang, Z. Ren, X.-J. Liu, and G.-B. Jo, *Nat. Phys.* **15**, 911 (2019).
- [37] X.-J. Liu, K. T. Law, and T. K. Ng, *Phys. Rev. Lett.* **112**, 086401 (2014).
- [38] J. Struck, J. Simonet, and K. Sengstock, *Phys. Rev. A* **90**, 031601 (2014).
- [39] M. L. Wall, A. P. Koller, S. Li, X. Zhang, N. R. Cooper, J. Ye, and A. M. Rey, *Phys. Rev. Lett.* **116**, 035301 (2016).
- [40] C. Zhang, S. Tewari, R. M. Lutchyn, and S. Das Sarma, *Phys. Rev. Lett.* **101**, 160401 (2008).
- [41] X.-J. Liu, M. F. Borunda, X. Liu, and J. Sinova, *Phys. Rev. Lett.* **102**, 046402 (2009).
- [42] C. Wang, C. Gao, C.-M. Jian, and H. Zhai, *Phys. Rev. Lett.* **105**, 160403 (2010).
- [43] M. Gong, S. Tewari, and C. Zhang, *Phys. Rev. Lett.* **107**, 195303 (2011).
- [44] D.-W. Zhang, Z.-Y. Xue, H. Yan, Z. D. Wang, and S.-L. Zhu, *Phys. Rev. A* **85**, 013628 (2012).
- [45] T. Ozawa and G. Baym, *Phys. Rev. Lett.* **110**, 085304 (2013).
- [46] Z. Zheng, M. Gong, X. Zou, C. Zhang, and G. Guo, *Phys. Rev. A* **87**, 031602 (2013).
- [47] Y. Deng, J. Cheng, H. Jing, and S. Yi, *Phys. Rev. Lett.* **112**, 143007 (2014).
- [48] Y. Xu and C. Zhang, *Phys. Rev. Lett.* **114**, 110401 (2015).
- [49] D.-W. Zhang, S.-L. Zhu, and Z. D. Wang, *Phys. Rev. A* **92**, 013632 (2015).
- [50] F. Sun, J. Ye, and W.-M. Liu, *Phys. Rev. A* **92**, 043609 (2015).
- [51] Y. Deng, T. Shi, H. Hu, L. You, and S. Yi, *Phys. Rev. A* **95**, 023611 (2017).
- [52] X. Zhou, J.-S. Pan, W. Yi, G. Chen, and S. Jia, *Phys. Rev. A* **96**, 023627 (2017).
- [53] X.-L. Chen, J. Wang, Y. Li, X.-J. Liu, and H. Hu, *Phys. Rev. A* **98**, 013614 (2018).
- [54] W. H. Tang and S. Zhang, *Phys. Rev. Lett.* **121**, 120403 (2018).
- [55] C.-H. Li, C. Qu, R. J. Niffenegger, S.-J. Wang, M. He, D. B. Blasing, A. J. Olson, C. H. Greene, Y. Lyanda-Geller, Q. Zhou, C. Zhang, and Y. P. Chen, *Nat. Commun.* **10**, 375 (2019).
- [56] Z. Lin, X.-J. Huang, D.-W. Zhang, S.-L. Zhu, and Z. D. Wang, *Phys. Rev. A* **99**, 043419 (2019).
- [57] Z. Zheng, Z. Lin, D.-W. Zhang, S.-L. Zhu, and Z. D. Wang, *Phys. Rev. Res.* **1**, 033102 (2019).
- [58] Y.-L. Chen, G.-Q. Zhang, D.-W. Zhang, and S.-L. Zhu, *Phys. Rev. A* **101**, 013627 (2020).
- [59] X. Shen, D.-W. Zhang, H. Yan, Z. Li, and S.-L. Zhu, *Phys. Rev. Res.* **2**, 013037 (2020).
- [60] B. Zhu, Y. Ke, H. Zhong, and C. Lee, *Phys. Rev. Res.* **2**, 023043 (2020).
- [61] J. Sánchez-Baena, J. Boronat, and F. Mazzanti, *Phys. Rev. A* **101**, 043602 (2020).
- [62] X.-L. Chen, X.-J. Liu, and H. Hu, *Phys. Rev. A* **106**, 023302 (2022).
- [63] L. Zhang and X.-J. Liu, *PRX Quantum* **3**, 040312 (2022).
- [64] Y.-Q. Zhu, Z. Zheng, G. Palumbo, and Z. D. Wang, *Phys. Rev. Lett.* **129**, 196602 (2022).
- [65] H. Li and W. Yi, *Phys. Rev. A* **107**, 013306 (2023).
- [66] L. Xiong, M. Gong, Z.-X. Fang, and R. Sun, *Chin. Phys. Lett.* **40**, 127402 (2023).
- [67] D. L. Campbell, R. M. Price, A. Putra, A. Valdés-Curiel, D. Trypogeorgos, and I. B. Spielman, *Nat. Commun.* **7**, 1 (2016).
- [68] X.-Y. Mai, Y.-Q. Zhu, Z. Li, D.-W. Zhang, and S.-L. Zhu, *Phys. Rev. A* **98**, 053619 (2018).
- [69] J. Hou, H. Hu, and C. Zhang, *Phys. Rev. A* **101**, 053613 (2020).
- [70] S. K. Adhikari, *Phys. Rev. A* **103**, L011301 (2021).
- [71] J. Cabedo, J. Claramunt, and A. Celi, *Phys. Rev. A* **104**, L031305 (2021).
- [72] Y. Chen, H. Lyu, Y. Xu, and Y. Zhang, *New J. Phys.* **24**, 073041 (2022).
- [73] Y. Su, J. Hou, and C. Zhang, *Phys. Rev. B* **107**, 085410 (2023).
- [74] P. Banger, Rajat, A. Roy, and S. Gautam, *Phys. Rev. A* **108**, 043310 (2023).
- [75] Y. Xu, Y. Chen, and X. Chen, *Phys. Rev. A* **109**, 063310 (2024).
- [76] S. K. Gangwar, R. Ravisankar, H. Fabrelli, P. Muruganandam, and P. K. Mishra, *Phys. Rev. A* **109**, 043306 (2024).
- [77] Y. A. Bychkov and E. I. Rashba, *J. Phys. C: Solid State Phys.* **17**, 6039 (1984).
- [78] G. Dresselhaus, *Phys. Rev.* **100**, 580 (1955).
- [79] X.-L. Qi, T. L. Hughes, and S.-C. Zhang, *Phys. Rev. B* **78**, 195424 (2008).
- [80] C. Cohen-Tannoudji, J. Dupont-Roc, and G. Grynberg, *Atom—Photon Interactions* (Wiley Online Library, 1998).